Available online at www.sciencedirect.com
SCIENCE DIRECT
International Journal of Machine Tools & Manufacture 45 (2005) 1329–1336
INTERNATIONAL JOURNAL OF MACHINE TOOLS & MANUFACTURE DESIGN, RESEARCH AND APPLICATION
www.elsevier.com/locate/ijmactool

Simulation of surface grinding process, part 2: interaction of the abrasive grain with the workpiece

T.A. Nguyen*, D.L. Butler

Center for Advanced Numerical Engineering Simulations, School of Mechanical and Production Engineering, Nanyang Technological University, Singapore 639798, Singapore

Received 5 July 2004; accepted 13 January 2005
Available online 22 February 2005

Abstract

This paper is the second part of the two-part series, which describes the kinematic simulation of the grinding process. The complex wheel–workpiece interaction is taken into consideration in the generation of the workpiece surface. An algorithm is proposed to identify the active abrasive grains and their attack angles from the wheel topography. Based on the critical values of the attack angle, the abrasive grain is determined either to cut, plough or rub the workpiece. A numerical example is used to validate the approach.

Keywords: Grinding; Simulation; Wheel topography

1. Introduction

Although the grinding process has been a topic of extensive research for the last 20 years, a complete understanding of the process has yet to be achieved. It is partly due to the fact that grinding is a stochastic process in that a large number of abrasive grains of random-defined geometry act as a cutting tool. The workpiece surface texture can be considered as the result of the summation of individual grain action. It is often believed that grinding involves cutting, ploughing and rubbing of the abrasive grains at the workpiece surface [1]. In fact, the nature of this interaction is very complex depending on various factors involved the grinding wheel, the workpiece, the machine and the process setting.

A realistic simulation requires that the wheel–workpiece interaction is correctly modelled. However, most of the suggested simulation schemes only considered the cutting action of the grains, neglecting ploughing and rubbing [2–6]. Chen and Rowe [7] made a significant advance for the technique by considering the side flows of the material in their work, but ploughing and rubbing of the grains were still neglected. Cooper and Lavine [8] accounted for the ploughing and rubbing using an empirical function of the abrasive grain depth of cut.

In part 1, a numerical procedure for generating the grinding wheel topography has been proposed. In part 2, a method of simulating the grinding process is described. The generation of the workpiece surface is started with the generation of the grinding wheel surface. Then the 3D topographical data is mapped to the 3D surface texture of the workpiece using their kinematic relationship. An algorithm is proposed to identify the active abrasive grains and their attack angles, based on which the interaction modes of the abrasive grains and the workpiece are determined. The model input includes the wheel velocity v_s, the workpiece velocity v_w, the depth of cut a, the grinding wheel diameter d_s and the 2D-array of grinding wheel surface heights. The output of the model is another 2-D array of surface heights, this time representing the topography of the workpiece surface.

2. Grinding process kinematics

A kinematic relationship between the grinding wheel cutting edges and the workpiece surface is shortly

* Corresponding author. Tel.: +65 67904071; fax: +65 67904073.
E-mail address: nta@pmail.ntu.edu.sg (T.A. Nguyen).

0890-6955/$ - see front matter © 2005 Elsevier Ltd. All rights reserved.
doi:10.1016/j.ijmachtools.2005.01.006

Nomenclature

A_r	area of side ridge
a	depth of cut
a_1	actual depth of cut
d_g	mean diameter of abrasive grains
d_{ij}	distance from cutting edge to the centre of a grinding wheel
d_s	nominal grinding wheel diameter
g_{mn}	workpiece surface topography
h	perpendicular bisector (or median) of triangle
h_{ij}	grinding wheel topography
k_a	contact stiffness
k_c	cutting stiffness
k_e	effective stiffness
k_m	machine stiffness
l	base side of a triangular side ridge
R	radius of grain tip
r	grain depth of cut
r_{ij}	distance in z coordinate between the local and global coordinate origins O',O
v_s	wheel velocity
v_w	workpiece velocity
α	attack angle of cutting edge
α_p	critical attack angle, smaller than which a cutting edge will only plough
α_r	critical attack angle, smaller than which a cutting edge will only rub
β	cutting efficiency ratio
θ	rotation angle of grinding wheel
ΔL_{ij}	peripheral distance of cutting point h_{ij}
Δx_s	sampling step between rows of grinding wheel topographic array $[h_{ij}]$
Δx_w	sampling step between rows of workpiece topographic array $[g_{ij}]$
κ	summit curvature

described. Based on the relationship, the equations for mapping the grinding wheel topography to workpiece surface texture are presented.

2.1. Cutting point trajectory equation

A detailed grinding kinematic analysis can be found in Malkin [9]. If a $O'xyz$ coordinate system is set with its origin O' fixed on the workpiece and coinciding with the grain at the lowest point (Fig. 1) the cutting path $FO'F'$ of the cutting point is a trochoid formed by the superposition of the circular motion around the wheel centre at velocity v_s and tangential motion along the workpiece at velocity v_w. The equations for the trochoid path are described as follows

$$x = \frac{d_s}{2}\sin\theta \pm \frac{d_s v_w}{2v_s}\theta \tag{1a}$$

$$z = \frac{d_s}{2}(1-\cos\theta) \tag{1b}$$

where x and z are the coordinates of grain G, v_w is the velocity of the workpiece, d_s is the nominal diameter of the grinding wheel, and θ is the rotation angle of the wheel. The plus sign in the equation refers to up-grinding, and the negative to the down-grinding with the workpiece velocity in the opposite direction. Since θ is a very small angle, the trochoid cutting path can be approximated by a parabola:

$$z = \frac{x^2}{\left[d_s\left(1 \pm \frac{v_w}{v_s}\right)^2\right]} \tag{2}$$

Similarly, the trajectory of each cutting edge on the grinding wheel surface (Fig. 2) can be expressed as

$$z_{ij} = \frac{x_{ij}^2}{\left[d_{ij}\left(1 \pm \frac{v_w}{v_s}\right)^2\right]} \tag{3}$$

where x_{ij} and z_{ij} are the coordinate of the cutting edge relative to the an x and z local coordinate system with the origin O', d_{ij} is the distance from cutting edge to the centre of the grinding wheel. d_{ij} can be estimated by the following equation

$$d_{ij} = d_s + h_{ij} \tag{4}$$

with d_s is the nominal diameter of the grinding wheel, and h_{ij} is the grinding wheel surface height relative to the nominal grinding wheel diameter. h_{ij} can be obtained from grinding wheel topography.

2.2. Mapping of cutting point trajectories to workpiece surface

All kinematic-based simulations of the grinding process require some schemes of mapping the cutting path to

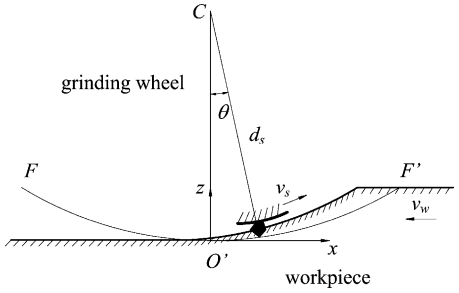

Fig. 1. Cutting point trajectory.

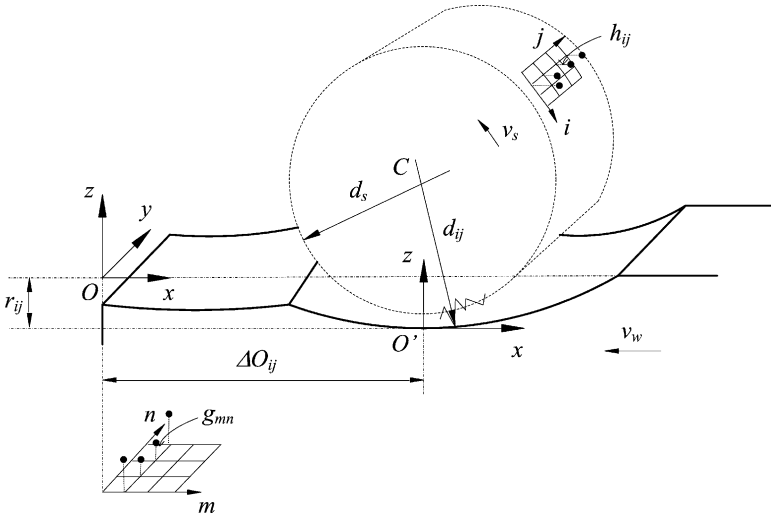

Fig. 2. Mapping of the cutting point trajectories to the workpiece surface.

the workpiece surface. The approach used in this paper is similar to other authors [2,6]. Suppose that the workpiece surface can be presented by a topographical array $[g_{ij}]$. Each member of g_{mn} of the array is defined in the global coordinate system $Oxyz$, with the indices m and n corresponding to the positions of the workpiece surface height g_{mn} in the x and y direction, respectively (Fig. 2). The origin O is selected so that

$$\max\{g_{mn}\} = 0 \tag{5}$$

Similarly, the grinding wheel topography can be described by an array of height $[h_{ij}]$ (Fig. 2) with the indices i and j corresponding to the positions of the topographical point h_{ij} in the peripheral and axial directions of the wheel, respectively. The position of the local origin O' of each cutting point relative to the global coordinate system can be estimated from the equation

$$\Delta O_{ij} = \frac{\Delta L_{ij} v_{\mathrm{w}}}{v_{\mathrm{s}}} \tag{6}$$

where ΔL_{ij} is the peripheral distance from the cutting point h_{ij} to the first cutting point. ΔL_{ij} can be estimated as

$$\Delta L_{ij} = i \Delta x_{\mathrm{s}} \tag{7}$$

with Δx_{s} is the step between rows of the grinding wheel topographic array $[h_{ij}]$ in the peripheral direction.

The trajectory of the cutting point, translated to the global coordinate $Oxyz$ is

$$z_{ij} = -r_{ij} + \frac{(x - \Delta O_{ij})^2}{\left[d_{ij}\left(1 \pm \frac{v_{\mathrm{w}}}{v_{\mathrm{s}}}\right)^2\right]} \tag{8}$$

where r_{ij} is the distance in z coordinate from the local coordinate origin O' to the global coordinate O. r_{ij} is equal to the actual depth of cut of the cutting point h_{ij}, which can be estimated as

$$r_{ij} = h_{ij} - h_{\max} + a \tag{9}$$

where $h_{\max} = \max\{h_{ij}\}$, and a is the specified depth of cut.

For each point mn of the workpiece topographic array the above equation can be written as

$$z_{mn} = r_{ij} + \frac{(m\Delta x_{\mathrm{w}} - \Delta O_{ij})^2}{\left[d_{ij}\left(1 \pm \frac{v_{\mathrm{w}}}{v_{\mathrm{s}}}\right)^2\right]} \tag{10}$$

where Δx_{w} is the distance between rows of the workpiece topographic array $[g_{ij}]$. Then, the workpiece topographic array can be updated as

$$g^i_{mn} = \min\{g^{i-1}_{mn}, z_{mn}\} \tag{11}$$

with g^{i-1}_{mn}, g^i_{mn} are the workpiece surface heights at point mn before and after the cutting point h_{ij} passes through.

3. Interaction of the abrasive grains and the workpiece surface

Depending on the grinding condition, only a small number of the abrasive grains on the grinding wheel will contact the workpiece surface. Among this small number of active grains, only a small portion will cut and form chips while the other will only plough or rub the workpiece surface. Therefore, an algorithm is first proposed to identify the active grain. Then, the attack angle of the active grain is estimated, based on which the grain will be determined to either cut, or plough, rub the workpiece surface.

3.1. Identification of abrasive grains

The active abrasive grains can be identified from the topographical array $[h_{ij}]$ by sliding the topography at

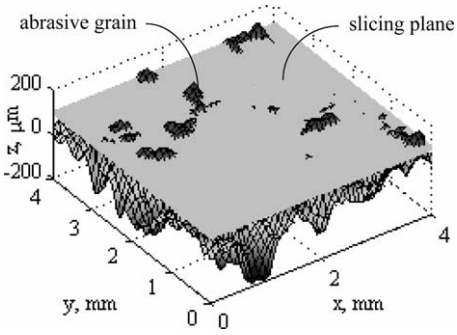

Fig. 3. Slicing plane.

the specified depth of cut a (Fig. 3) as follows

$$h_{ij} \geq h_{\max} - a \tag{12}$$

where $h_{\max} = \max\{h_{ij}\}$. Eq. (12) implies that the highest cutting point of $[h_{ij}]$ will cut the workpiece surface at the depth a.

The clusters of the topographical points remained on the grinding wheel topography can be classified as the active abrasive grains. Strictly speaking, these abrasive grains are only static active, as in the grinding process they may or may not contact the workpiece surface. In order to identify the active abrasive grain from the topographical array, a search algorithm is proposed. The search process starts with the first point of the abrasive grain (circle point in Fig. 4a). By searching the neighbourhood points of the circle point, the next search front is identified (all the rectangular points). The searching of all the neighbourhood points is repeated for the rectangular points for identifying the successive search front (all the triangular points). The process continues until all the adjacent points are identified.

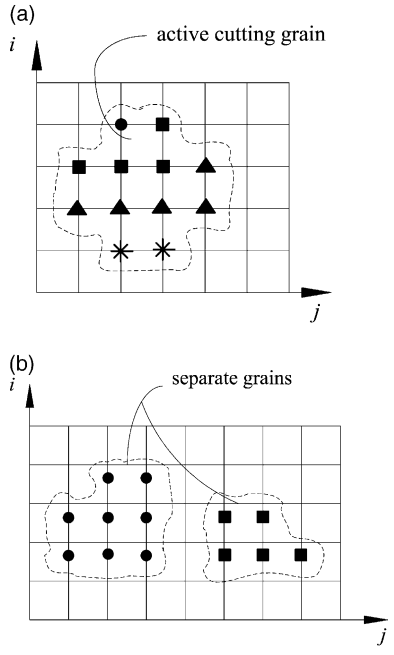

Fig. 4. Active grain identification.

All the found points are considered as belonged in the same abrasive grains. Strictly speaking, the two closely-positioned clusters of the cutting points can possibly belong to the same abrasive grain (Fig. 4b). This situation can be remedied by considering the distance between two clusters. If the distance is smaller than the average grain diameter, they can be considered as belonging to the same grain. However, in this simulation, two non-adjacent clusters are considered as two separated grains.

3.2. Attack angle of the abrasive grain

In grinding metals three distinct phases can be distinguished at the interface of the abrasive grain and the workpiece: rubbing, ploughing and cutting [1]. When the depth of cut is shallow, the grain only slides on the work causing elastic deformation in the work material with essentially no material removal. This is rubbing phase. Ploughing occurs as the grain causes more plastic flow of the work material in the direction of sliding with material being thrown up and broken off the sides of the groove.

Komanduri [10], carrying out single point turning with negative rake angle tools, found that the value of the rake angle decided whether the tool cut, ploughed or rubbed. Takenaka [11] observed that there was a critical depth of cut when the grain stopped cutting. Xie and Williams [12] studied abrasive wear by repeating sliding of a hard asperity on the workpiece surface. They established that the deformation modes of the material depended essentially on the following factors: lubrication, the mechanical properties of the softer material and the distance between adjacent tracks in repeated pass situation. Kato [13] conducted a scratch test in SEM apparatus, and observed that the material removal mode was affected by the degree of penetration, lubrication, and the hardness ratio of the abrading tip and the wear surface. Butler et al. [14] showed that the grinding performance was correlated with the arithmetic sum of the curvature of the grinding wheel surface.

The above review shows that attack angle of the cutting edge has certain influence on the interaction of the abrasive grain with workpiece. In this paper, the action of the abrasive grain is assumed to depend on the attack angle of the abrasive grain. It means that there exists a critical value α_p of attack angles at which the grinding action of the cutting edge will transit from cutting to ploughing. Similarly, the grinding action of the cutting edge will involve only rubbing action when its attack angle is smaller certain critical value α_r. Such critical values can be obtained from experimentation. If the abrasive grain tip is approximated as the sphere [15], the attack angle can be estimated as follows (Fig. 5)

$$\alpha = \arccos\left(\frac{R-r}{R}\right) \tag{13}$$

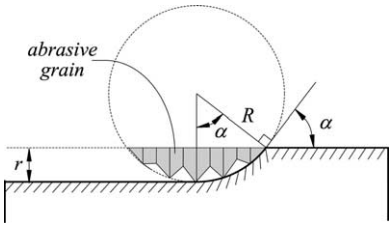

Fig. 5. Attack angle of an abrasive grain.

where R is the radius of a spherical tip, and r is the grain depth of cut. The radius of the abrasive grain tip can be found from the curvature of the grain. Since the sum of the curvatures of a surface at a point along any two orthogonal directions is equal to the sum of the principal curvatures [16]. The curvature of the abrasive grain can be defined as the arithmetic mean summit curvature of all the cutting points forming the abrasive grain

$$\kappa = -\frac{1}{2n} \times \sum_{k=1}^{n} \left(\frac{h_{i+1,j} + h_{i-1,j} - 2h_{ij}}{\Delta x_s^2} + \frac{h_{i,j+1} + h_{ii,j-1} - 2h_{ij}}{\Delta y_s^2} \right) \tag{14}$$

where n is the number of the cutting points forming the abrasive grain. i and j are the indices of the height point. Subsequently, the radius of the abrasive grain sphere is deduced as

$$R = \frac{1}{\kappa} \tag{15}$$

3.3. Update side flow profile

A portion of the displaced material, when the grains cut or plough, will remain on the workpiece surface and form side ridges along the groove. For the simulation, the cross section of the side ridges can be modelled as an isosceles triangle with base angle α equivalent to the attack angle of the abrasive grain. The size of the cross section can be estimated as follows (Fig. 6)

$$A_r = \frac{1}{2} hl \tag{16a}$$

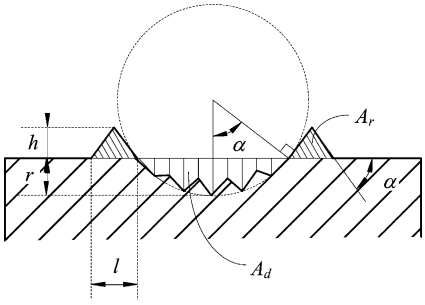

Fig. 6. Side ridges of grooves.

$$h = \sqrt{A_r tg\ \alpha} \tag{16b}$$

$$l = 2\sqrt{A_r \cot\ \alpha} \tag{16c}$$

where h is the perpendicular bisector (or median), l is the base side of the side ridge, and A_r is the area of the side ridge. The area A_r is proportional to the area of the groove by the cutting efficiency ratio β. The single grit scratch testing showed that the ratio could be varied from 70 to 100% for ploughing, and 10–50% for cutting. Similar approach was used by Chen and Rowe [7], except that a ridge is approximated as a parabola.

4. Simulation procedure

Fig. 7 shows the procedure for simulating the grinding process. The input for the simulation includes the samples of the wheel topography, wheel velocity v_s, workpiece velocity v_w, grinding wheel diameter d_s, and depth of cut a. The simulation procedure starts with the generation of the grinding wheel topography based on the sampled wheel data. The generated topographical array $[h_{ij}]$ is then sorted to identify the static active grains, together with the estimation of the radii of the grains. Using the given depth of cut a, wheel velocity v_s and workpiece velocity v_w the grinding wheel data $[h_{ij}]$ is mapped to the workpiece surface

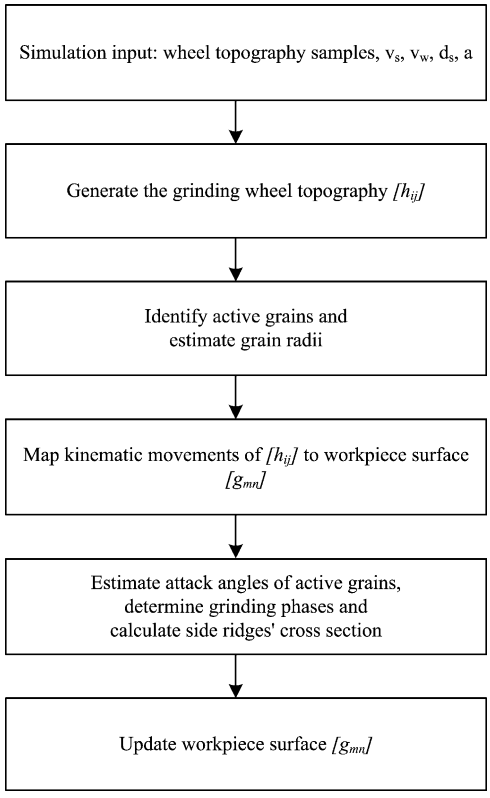

Fig. 7. Simulation procedure.

Table 1
3D surface characterization of the workpiece surface

Parameter		*Sq*	*Sz*	*Ssk*	*Sku*	*Str*	*Sal*	*Std*	*Sds*	*SΔq*	*Ssc*	*Sdr*	*Sbi*	*Sci*	*Svi*
Mild	*E*	0.78	4.71	−0.10	2.6	0.05	0.04	0	51.34	0.03	0.001	0.04	0.63	1.63	0.14
steel	*S*	1.05	5.39	−0.19	2.7	0.05	0.04	0	14.97	0.04	0.001	0.07	0.63	1.59	0.15
D2	*E*	0.34	2.26	−0.48	3.7	0.05	0.04	0	54.88	0.01	0.005	0.01	0.65	1.56	0.17
	S	0.39	2.41	−0.74	4.5	0.05	0.04	0	22.71	0.01	0.005	0.01	0.70	1.35	0.26

E, averaged experimental result; *S*, averaged simulation result.

texture [g_{mn}]. At each cross-section m of the workpiece surface [g_{mn}], the grain depth of cut and the area of the displaced workpiece material are found. Next, the attack angle of the active grain at the mth section of the workpiece surface is evaluated, based on which the grinding mode of the active grain (cutting, ploughing, or rubbing) is decided. The workpiece surface is updated by superimposing the grooving and side ridge cross section.

5. Model verification

For the purpose of model verification, two grinding experiments were conducted on an Okamoto 63DXV surface-grinding machine. The workpiece material is mild steel and tool steel D2. The spindle system was balanced by a microbalancer Okamoto MB-3. The amplitude of the wheel head vibration was adjusted to be less than 0.1 μm peak-to-peak at a maximum rotational speed of 1500 rpm.

The grinding wheel was aluminum oxide A80J8V and A80H8V. The wheel was trued with 30 μm depth of cut, 4 passes and a crossfeed velocity of 5 mm/s (0.2 mm/rev). Then it was dressed with 15 μm depth of cut, 2 passes and a crossfeed velocity of 2.5 mm/s (0.1 mm/rev). For the case of grinding D2 workpiece, two additional idle passes were carried out following the dressing operation. After dressing, the wheel surface was replicated at 4 locations, and its topography was captured using Talyscan 150 3D stylus measuring system. The sampling interval was 40 μm and the stylus speed was 0.3 mm/s.

The workpiece of mild steel was first ground flat with 20 μm down-feed set on the grinding machine. A layer of 0.2 mm was removed. Then, it was finished with 10 μm downfeed. For the D2 workpiece, a layer of 0.3 mm was removed with 20 μm down-feed set on the grinding machine. Then, it was ground with 10 μm downfeed with 5 grinding passes. The last 5 passes were carried out at 5 μm downfeed. Four samples of the topography for each workpiece were taken by Talyscan 150 system.

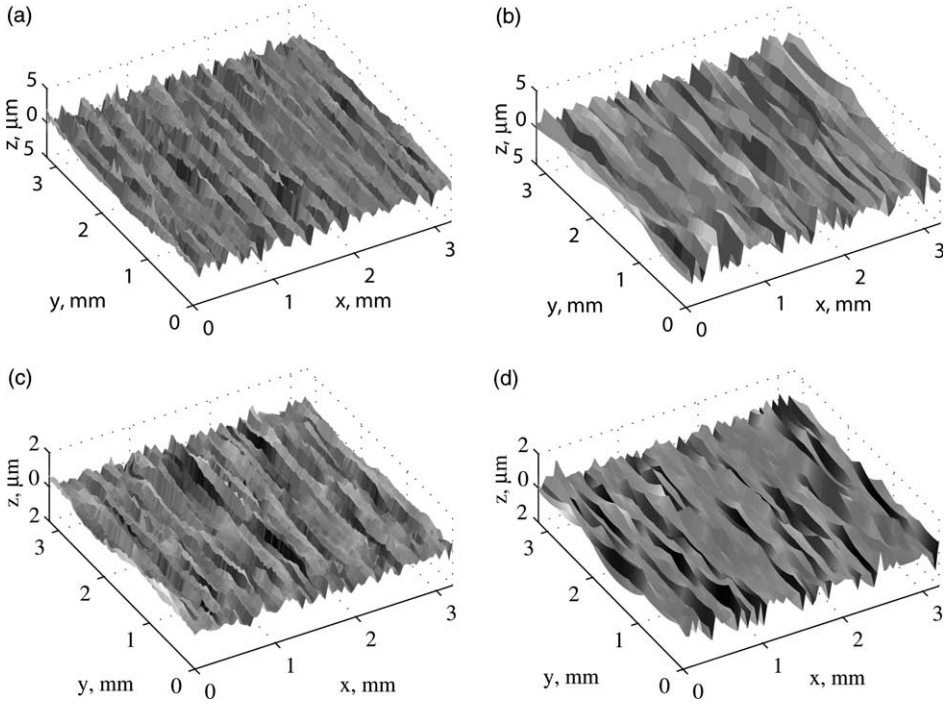

Fig. 8. The topography of the workpiece surfaces. (a) mild steel experimental surface; (b) mild steel simulated surface; (c) D2 experimental surface; (d) D2 simulated surface.

It was crucial to decide the sampling interval as the grinding action of one grain in the model is determined based on the grain curvature. It has been shown that the sampling interval has a significant effect on the characterization of the grinding wheel [17]. By varying the sampling interval, either cutting edges or grains of the grinding wheels can be characterized. Verkerk [18] proposed that although there are numerous cutting edges on an abrasive grain, they could be considered to behave as one cutting edge. For general measurement of active grains, it is considered that the optimum sampling interval ss_{opt} required to measure active grain should fulfill the following relationship [17]:

$$3 \leq \frac{d_g}{ss_{opt}} \leq 4 \tag{17}$$

where d_g is the mean diameter of abrasive grains, which can be estimated as [9]

$$d_g(\text{mm}) = 28\, M^{-1.1} \tag{18}$$

with M is the mesh number of the grinding wheel.

The critical attack angles α_p and α_r for this grinding condition were chosen based on the equation suggested by Xie and Williams [12]. For mild steel, α_p is roughly 25.5° and α_r is about 1°. Another important input is the actual depth of cut used in the simulation. Due to the deflection of the machine, workpiece and grinding wheel, the actual depth of cut may be far from the down-feed set on the grinding machine. The actual depth of cut can be approximated from the ground grooves on the workpiece surface or from the following Eq. [9]:

$$a_1 = \frac{a}{1 + \frac{k_c}{k_e}} \tag{19}$$

where a_1 is the actual depth of cut, a is the depth of cut set on the grinding machine, k_c is the cutting stiffness, and k_e is the effective stiffness, estimated as

$$\frac{1}{k_e} = \frac{1}{k_m} + \frac{1}{k_a} \tag{20}$$

with k_m is the machine stiffness and k_a is the contact stiffness. The range of stiffness k_c, k_m, and k_a found in grinding are: $k_m = 10$–100 kN/mm; $k_c/b = 2$–10 kN/mm^2; $k_a/b = 1$–10 kN/mm^2.

The simulation was run on the PC Pentium II-500 MHz. A total of 4 simulations were conducted. Computer time for one simulation was approximately 10 min. The averaged 3D characterization parameters workpiece surface, obtained from the experiment and the simulation is given in Table 1. A comparison between the two data sets shows that amplitude (*Sq*, *Sz*, *Ssk* and *Sku*), autocorrelation (*Str*, *Sal*, *Std*) and functional (*Sbi*, *Sci*, *Svi*) parameters are in good agreement while other parameters (*Sds* and *Sdr*) show larger variation. These variations can be explained by the fact that the parameters are strongly influenced by frequency components of the surface texture. The simulated surface however has less high frequency components compared to the real surface. The topography of the ground workpiece and the simulated surface is shown in Fig. 8, which clearly resemble each other.

6. Conclusions

A numerical procedure is proposed for the kinematic simulation of the grinding process. The method takes into consideration the complex nature of the wheel–workpiece interaction by assuming that the attack angle of the abrasive grain will decide the interaction mode. An algorithm is proposed for the estimation of the attack angle using the summit curvature of the topographical point. The workpiece surface is updated according to the estimated material removal mode. The agreement between the simulated and experimental result shows that the method proves the effectiveness of the method.

References

[1] R.S. Hahn, R.P. Lindsay, Principles of grinding part 1: basic relationships in precision grinding, in: C. Bhateja, R. Lindsay (Eds.), Grinding Theory Techniques and Troubleshooting, SME, Michigan, 1982, pp. 3–10.
[2] X. Zhou, F. Xi, Modelling and predicting surface roughness of the grinding process, International Journal of Machine Tools & Manufacture 42 (8) (2002) 967–977.
[3] G. Warnecke, U. Zitt, Kinematic simulation for analyzing and predicting high-performance grinding processes, Annals of CIRP 47 (1) (1998) 265–270.
[4] I. Inasaki, Grinding process simulation based on the wheel topography measurement, Annals of CIRP 54 (1) (1996) 347–350.
[5] Y. Wang, K.S. Moon, A methodology for the multi-resolution simulation of grinding wheel surface, Wear 211 (2) (1997) 218–225.
[6] E.J. Salisbury, K.V. Domala, K.S. Moon, M.H. Miller, J.W. Sutherland, A three-dimensional model for the surface texture in surface grinding, part 2: grinding wheel surface texture model, Journal of Manufacturing Science and Engineering 123 (4) (2001) 582–590.
[7] X. Chen, W.B. Rowe, Analysis and simulation of the grinding process, part 2: mechanics of grinding, International Journal of Machine Tools and Manufacture 36 (8) (1996) 883–896.
[8] W. Cooper, A.S. Lavine, Grinding process size effect and kinematics numerical analysis, Journal of Manufacturing Science and Engineering 122 (1) (2000) 59–69.
[9] S. Malkin, Grinding Technology: Theory and Applications of Machining with Abrasives, Ellis Horwood, Chichester, 1989.
[10] R. Komanduri, Some aspects of machining with negative rake tools simulating grinding, International Journal of Machine and Tool Design Research 11 (1971) 223–233.
[11] N. Takenaka, A study on the grinding action by single grit, Annals of CIRP 13 (1) (1966) 183–190.

[12] Y. Xie, J.A. Williams, The prediction of friction and wear when a soft surface slides against a harder rough surface, Wear 196 (1) (1996) 21–34.
[13] K. Kato, Micro-mechanisms of wear–wear modes, Wear 153 (1) (1992) 277–295.
[14] D.L. Butler, L.A. Blunt, B.K. See, J.A. Webster, K.J. Stout, The characterisation of grinding wheels using 3d surface measurement techniques, Journal of Materials Processing Technology 127 (2) (2002) 234–237.
[15] M.C. Shaw, Principles of Abrasive Processing, Clarendon Press, Oxford, 1995.
[16] K.J. Stout, P.J. Sullivan, W.P. Dong, E. Mainsah, N. Luo, T. Mathia, H. Zahouani, The development of methods for the characterisation of roughness in three dimensions, Commission of European Communities Luxembourg 1993;.
[17] L. Blunt, S. Ebdon, The application of three-dimensional surface measurement techniques to characterising grinding wheel topography, International Journal of Machine Tools and Manufacture 36 (11) (1996) 1207–1226.
[18] J. Verkerk, Final report concerning CIRP cooperative work on the characterization of grinding wheel topography, Annals of CIPR 26 (2) (1977) 385–395.